Title	Preparation of oriented ZnO rod arrays using hexagonal plate-like particles as a seed layer
Author(s)	Koyasu, Satoshi; Makino, Hiroki; Tarutani, Naoki; Suzuki, Tohru; Uchikoshi, Tetsuo; Ishigaki, Takamasa
Citation	Langmuir , 39 (1) : 487 - 494
Issue Date	2022-12-27
DOI	10.1021/acs.langmuir.2c02734
Self DOI	
URL	https://ir.lib.hiroshima-u.ac.jp/00053530
Right	© 2022 American Chemical Society This document is the Accepted Manuscript version of a Published Work that appeared in final form in Langmuir, copyright © American Chemical Society after peer review and technical editing by the publisher. To access the final edited and published work see https://doi.org/10.1021/acs.langmuir.2c02734 This is not the published version. Please cite only the published version. この論文は出版社版ではありません。引用の際には出版社版をご確認、ご利用ください。
Relation	


Hiroshima University Institutional Repository

Preparation of oriented ZnO rod arrays using hexagonal plate-like particles as a seed layer

Satoshi Koyasu(1), Hiroki Makino(1), Naoki Tarutani(2)(3), Tohru Suzuki(4), Tetsuo Uchikoshi(3)(4), Takamasa Ishigaki*(1)(3)

(1) Department of Chemical Science and Technology, Hosei University, 3-7-2 Kajino-cho, Koganei, Tokyo 184-8584, Japan

(2) Graduate School of Advanced Science and Engineering, Hiroshima University, 1-4-1 Kagamiyama, Higashi-Hiroshima, Hiroshima 739-8527, Japan

(3) Research Center for Micro-Nano Technology, 3-11-15 Midori-cho, Koganei, Tokyo 184-0003, Japan

(4) Research Center for Functional Materials, National Institute for Materials Science (NIMS), 1-2-1 Sengen, Tsukuba, Ibaraki 305-0047, Japan

*Corresponding author: ishigaki@hosei.ac.jp

ABSTRACT

ZnO rod film is a promising material for electrodes and sensors due to its large surface area and high electrical conductivity. One of the drawbacks of conventional ZnO rod film is the random orientation of rods. In this study, an oriented ZnO seed layer composed of hexagonal plate-like ZnO particles was prepared by dip-coating. An oriented ZnO rod film was then synthesized by growing this seed layer using a hydrothermal synthesis method. We optimized the concentration of the precursor and the hydrothermal treatment time to synthesize homogeneous ZnO rod arrays. The uniformity of the rod arrays was improved by applying a strong magnetic field (12 T) during hydrothermal treatment.

1. Introduction

Zinc oxide (ZnO) is an n-type semiconductor with a bandgap of 3.37 eV (10 K) [1] or 3.3 eV (room temperature) [2] and a wurtzite structure. The piezoelectric and pyroelectric properties of ZnO are derived from the symmetry of P63mc. [3] As a result of these properties, ZnO can be used as a SAW filter [4] and piezo actuator. [5] Reported electron mobility of ZnO is 200 cm^2/Vs (synthesized by hydrothermal method)[6], 155 cm^2/Vs (PLD)[7], 130 cm^2/Vs (MBE)[8], 440 cm^2/Vs (PLD)[9]. These values are relatively high for an oxide semiconductor. Doping aluminum into ZnO increases conductive electrons and improves conductivity. This material (Al-doped ZnO) is called AZO[10,11] and is known as a typical transparent conductive oxide (TCO)[12] along with indium tin oxide (ITO)[13] and fluorine-doped tin oxide (FTO)[14–16]. Although ZnO normally exhibits n-type behavior, nitrogen, and aluminum co-doped ZnO exhibits p-type behavior.[17] Due to the high transparency and mobility of ZnO, it is used as transparent conductive film[18], thin film transistor [19], and solar cell material [20,21]. Furthermore, when flammable gas is adsorbed on the surface of ZnO, electrons are donated to the conduction band of ZnO, and the electric conductivity changes. For these reasons, ZnO is used as a semiconductor-type gas sensor. [22–24] The advantage of ZnO is that it is less expensive than tin oxide (SnO_2) [25] when used for a semiconductor gas sensor.

ZnO particles take various shapes depending on the method used to synthesize them. Hexagonal plate [26], spindle [27], donut [28], hexagonal columnar, hexagonal pyramid, wire, urchin [29], and sphere [30,31] shaped particles have been synthesized thus far. The flexible shape of ZnO is useful for its applications. For example, when ZnO is used as a gas sensor or catalyst support, rod-shaped ZnO is advantageous due to its large surface area. In another case, it has been reported that ZnO rods and Poly(3-hexylthiophene-2,5-diyl) (P3HT) make a bulk heterojunction structure with excellent

properties as photovoltaic devices.[32–34] Other than ZnO rods/P3HT, photovoltaic devices using ZnO rods/metal-organic perovskites[35] and ZnO rods/cadmium sulfide[36] have been reported.

ZnO needs to be fixed on a substrate in order to be applied to electrodes and sensors. In particular, ZnO rod arrays formed on the substrate have attracted attention due to their large surface area and high electroconductivity. The following methods are used to grow ZnO directly from a substrate. ZnO rods with a diameter of 80 to 120 nm and a length of 10 to 20 μm can be synthesized by vapor phase growth using gold nanoparticles fixed on a substrate as a catalyst.[37] A ZnO rod with a thickness of 20 nm and a diameter of about 400 nm can be synthesized by a hydrothermal synthesis method using polycrystalline ZnO film as a seed.[38] When these synthetic methods are used, ZnO grows in random directions from gold particles and polycrystalline ZnO, and it is difficult to construct a ZnO array with controlled crystal orientation.

In this study, we prepared a seed layer in which hexagonal plate ZnO particles were regularly arranged on a substrate. Then, an oriented ZnO rod was grown on the seeded layer. ZnO particles were arranged regularly by preparing two-dimensional colloidal crystals of hexagonal plate-like ZnO particles. Two-dimensional colloidal crystals are monodispersed particles arranged on a substrate with translational symmetry. These colloidal crystals have been produced by dip-coating dispersions of silica or polystyrene spherical particles onto clean substrates.[39,40] Two main driving forces for the growth of two-dimensional colloidal crystals have been identified. One is the flow of solvent generated by the evaporation of solvent from two-dimensional colloidal crystals. The other is an attractive force known as the lateral capillary force generated between particles via surface tension.[41,42] Because this method can control the diameter of the rod by changing the size of the particles used for the seed, it is possible to synthesize ZnO rods of various shapes on the substrate.

We used a hydrothermal synthesis method to grow ZnO rods and investigated the effects of reaction time and precursor concentration on the rod shape. Although zinc nitrate is often used as a raw material for synthesizing ZnO rods via the hydrothermal synthesis method,[43–46] we used zinc hydroxide as a raw material to eliminate the effect of counter ions. For stable crystal growth, hydrothermal treatment was performed even in a high magnetic field. A method of growing a crystal by the Czochralski method in a magnetic field can be used to grow a single crystal of silicon.[47] In this method, convection is suppressed by a high magnetic field and the temperature distribution becomes homogeneous so that a homogeneous single crystal can be produced. Suppression of convection by a high magnetic field has been also reported in an aqueous solution.[48] In our study, we applied this method of crystal growth in a magnetic field to the hydrothermal synthesis method to control the shape of the ZnO rod. ZnO is not a magnetic material but has a very weak diamagnetic anisotropy. It has been reported that when cast molding is performed in a high magnetic field, a green body can be obtained in which the c-axis is oriented perpendicular to the rotating magnetic field.[49] In addition, it has been reported that when non-magnetic metal bismuth is vapor-deposited in a strong magnetic field, a crystal film oriented in the magnetic field direction can be obtained. [50] This means that the orientation of the crystal nuclei is affected by the magnetic field when particles are heterogeneously nucleated on the substrate. In our case, the magnetic field may also cause the formation of crystal nuclei with an orientation different from that of the seed crystal. In this study, we also investigated whether the orientation of ZnO rods changes in response to a high magnetic field.

2. Experimental method

2.1 Fabrication of ZnO seed layer

The ZnO seed layer was formed on the indium tin oxide (ITO) coated glass substrate (12 mm×12 mm) as the foundation of the ZnO rod arrays. Hexagonal plate-like ZnO particles XZ-1000F-LP (Figure 1) manufactured by Sakai Chemical Industry Co., Ltd. (Osaka, Japan) were used as seed particles. Typical diameters and thicknesses of hexagonal plate-like particles are about 1000 nm and 200 nm, respectively, including some small particles. Ethanol (FUJIFILM Wako Pure Chemical Corporation, Osaka, Japan), polyethyleneimine (FUJIFILM Wako Pure Chemical Corporation, Osaka, Japan, molecular weight: 10000), and hexagonal plate ZnO particles were placed in a beaker so that the total volume was 10 mL. A ZnO dispersion was prepared by repeating ultrasonic irradiation (300 W, 20 kHz) for 3 minutes and a 2-minute stop cycle ten times each in an ice bath using an ultrasonic homogenizer (US-300T: NIHONSEIKI KAISHA LTD., Tokyo, Japan). The concentration of ZnO particles were 1, 7.5, and 10 vol% with respect to the solvent. The amount of polyethyleneimine added was 0.3% with respect to ZnO.

Next, the ZnO dispersion and ITO glass were set in a dip-coater (ND-0407-S5: SDI Company Ltd., Kyoto, Japan), and dip-coating was performed at a withdrawal speed of 5 μm/s. A ZnO seed layer was prepared by heating this substrate at 200 ℃ for 10 min. To investigate the effect of the withdrawal speed on the morphology of the seed layer, the ZnO concentration was fixed at 10 vol.%, and dip-coating was performed at withdrawal speeds of 5, 10, 100, 1000 μm/s.

2.2 Synthesis of zinc hydroxide

Zinc hydroxide was synthesized as a counter ion-free precursor used for the crystal growth of ZnO. 5.0 g of zinc nitrate hexahydrate($Zn(NO_3)_2 \cdot 6H_2O$: FUJIFILM Wako Pure Chemical Corporation, Osaka, Japan) was dissolved in 500 mL of distilled water to prepare an aqueous zinc nitrate solution. 28 wt% ammonia solution (FUJIFILM Wako Pure Chemical Corporation, Osaka,

Japan) was added dropwise until the pH of the aqueous zinc nitrate solution reached 7.6 to obtain a white precipitate. The obtained precipitate was filtered and then dried at 55 °C for 2 hours to obtain a powder sample.

2.3 Fabrication of ZnO rod arrays by hydrothermal method

Hydrothermal treatment was conducted to fabricate ZnO rod arrays from the seed layer. The zinc hydroxide obtained in section 2.2 was added to 35 mL of distilled water so that the zinc concentration became 0.02, 0.05, and 0.1 mmol/L, and ammonia solution was added to adjust the pH to 11. This suspension and the ZnO seed layer prepared in section 2.1 were placed in a stainless steel/Teflon autoclave container (volume 50 mL) and subjected to hydrothermal treatment at 120 °C for 0.5, 3, 6, and 12 hours. The substrate was placed with the seed layer facing down. After the hydrothermal treatment, the substrate was washed with distilled water, and SEM observation and XRD measurement were performed.

2.4 Effect of magnetic field on hydrothermal treatment

To investigate the effect of the magnetic field, hydrothermal treatment was performed on the ZnO seed layer in a superconducting magnet (JMTD12T100NC5, Japan Superconductor Tech. Inc., Kobe, Hyogo, Japan). Figure 2 shows a schematic illustration of a hydrothermal treatment facility in a strong magnetic field. In this experiment, a small brass/Teflon autoclave (volume of 20 mL) was used to insert into a superconducting magnet. The zinc hydroxide obtained in section 2.2 was added to 15 mL of distilled water so that the zinc concentration became 0.1 mmol/L, and ammonia solution was added to adjust the pH to 11. This suspension and the ZnO seed layer prepared in section 2.1 were placed in an autoclave container, and hydrothermal treatment was

performed at 120 °C for 3 hours while applying a magnetic field of 12 T. The direction of application of the magnetic field was perpendicular or horizontal with respect to the substrate. After the hydrothermal treatment, the substrate was washed with distilled water, and SEM observation was performed.

3 Results and discussion

3.1 Optimization of dip-coating condition

Figure 3 shows SEM images of dip-coated ZnO films prepared from a suspension with a ZnO volume fraction of 1, 7.5, and 10% at a withdrawal speed of 5 μm/s. When the particle concentration was 1 vol.%, the particle density on the substrate was low. The particle density on the substrate increased as the particle concentration of the suspension increased. The highest density ZnO film was obtained when a suspension with a particle concentration of 10 vol.% was used.

The following equation demonstrates that when the volume fraction of the particles in the solution is low, the packing density also becomes small.

According to Nagayama et al., the growth rate v_c of the two-dimensional colloidal crystal film can be represented by the following equation, [51]

$$v_c = \frac{\beta l j_e \varphi}{h(1-\epsilon)(1-\varphi)}. \qquad \text{(Eq. 1)}$$

Here, β is the ratio of the flow velocity of water to the particles, l is the evaporation range width of the particle film growth point, j_e is the solvent evaporation rate near the film growth, φ is the volume fraction of the particles, h is the film thickness, and ε is the porosity of the film. The following Eq. 2 is a modification of Eq. 1 focusing on the packing density (1-ε),

$$(1-\epsilon)=\frac{\beta l j_e}{h v_c}\frac{\varphi}{1-\varphi}. \qquad \text{(Eq. 2)}$$

The predictions from these equations are consistent with the results of the experiment.

Figure 4 shows SEM images of ZnO seed layers formed with the suspension concentration fixed at 10 vol.% and the dip-coat withdrawal speeds set to 5, 10, 100, and 1000 μm/s. The hexagonal plate ZnO particles appeared to have a close-packed structure in samples with a withdrawal speed of 5 and 10 μm/s, but the particles accumulated sparsely and irregularly when the withdrawal speed was 100 and 1000 μm/s. When the withdrawal speed is high, the transport of particles derived from the solvent flow cannot follow the withdrawal speed. Therefore, the particle density on the substrate decreases, and an irregular deposition of particles occurs because there is not enough time for the particles to rotate and settle in the most stable position. Figure 5 shows the XRD pattern of the ZnO seed film formed with withdrawal speeds of 5, 10, 100, and 1000 μm/s. Because the diffraction peak on the 002 plane of ZnO was strong at all withdrawal speeds, the c-axis of the ZnO particles was oriented perpendicular to the substrate. When the sample withdrawal speed is low, peaks other than the 002 plane, such as the 100 and 101 planes, become smaller. Figure 6 shows the degree of orientation of each sample evaluated by the Lotgering factor. Lotgering factor *F* was calculated by the following Eq. 4 using the diffraction intensity ratio ρ (Eq. 3) of the 00*l* plane of the sample and the diffraction intensity ratio ρ_0 of the 00*l* plane of the non-oriented ZnO.[52]

$$\rho=\frac{\sum_l I(00l)}{\sum_{hkl} I(hkl)}. \qquad \text{(Eq. 3)}$$

$$F=\frac{\rho-\rho_0}{1-\rho_0}. \qquad \text{(Eq. 4)}$$

To prepare a highly oriented film, the withdrawal speed should be as low as possible, and the optimal results were obtained specifically at 5 μm/s. In the sample prepared at 5 μm/s, the *F* value was 0.98, which was close to a perfect orientation. Even the sample prepared at the withdrawal speed of 1000 μm/s, which has the lowest degree of orientation, showed a high degree of orientation with an F value of 0.89.

3.2 Effect of hydrothermal treatment time on rod shape

A ZnO rod array was obtained by hydrothermal synthesis using hexagonal plate ZnO as a seed crystal. The crystallographic direction of the ZnO rods was the same as that of the seed crystals, and the c-axis was perpendicular to the substrate. Figure 7 shows an SEM image of a sample with the duration of hydrothermal treatment from 30 minutes to 12 hours. At the initial stage of the reaction, only the edge of the seed crystal grew, and the central part of the seed crystal was filled subsequently. On the contrary, crystal growth was not observed in the in-plane direction of the substrate (a b-axis direction) in any of the samples. The initial thickness of the seed layer was 0.2 μm, and the thickness became 1.4 μm after 3 hours of crystal growth. Figure 8 shows a plot of the ZnO film thickness against the hydrothermal treatment time. The crystal growth was completed within 3 hours from the start of hydrothermal treatment, and there was almost no change in thickness after that.

In the early stages of hydrothermal synthesis, only the edges of the ZnO rods grew, which are known as hollow crystals or hopper crystals. [53,54] Hopper crystals form as a result of the Mullins-Sekerka instability [55] and when crystal growth is diffusion controlled. This shape is obtained because the Zn or O atoms cannot be supplied to the concave portion and the growth occurs only in the convex portion. From the middle to late stages of hydrothermal synthesis, the supersaturation

decreases, and the crystal precipitation rate slows down. Then, the uptake of atoms on the surface becomes the rate-determining factor for crystal growth, and the cavity disappears. Growth in the in-plane direction of the substrate did not take place, suggesting that the hollow crystal fills from the bottom surface instead of from the walls.

3.3 Effect of precursor concentration on rod shape

To investigate the effect of the precursor concentration on the shape of the ZnO rod, the hydrothermal treatment time was fixed at 6 hours. Figure 9 shows SEM images of the top view and cross-section of the ZnO rod array films synthesized at precursor concentrations of 0.02, 0.05, and 0.1 mmol/L.

Hollow crystal rods were generated when the precursor concentration was 0.02 mmol/L, and solid crystal rods were generated when the precursor concentration was 0.05 and 0.1 mmol/L. Thus, a concentration of 0.05 mmol/L or more is required to form a solid ZnO rod.

Under the precursor concentration of 0.05 mmol/L or more, the film thickness was constant regardless of the concentration of the precursor. This is because the raw material was consumed in a place other than the substrate and deposited as ZnO particles in the solution. In the initial stage of the hydrothermal reaction, the supersaturation of ZnO rapidly increased, and homogeneous nucleation occurred in the solution. The higher the concentration of the raw material, the more crystal nuclei were generated by homogeneous nucleation, and the raw material was consumed for the growth of crystals in the solution.

3.4 Effect of magnetic field

Figure 10 shows SEM images of ZnO rod arrays synthesized in a magnetic field of 12 T. Figure 10 (a) is grown arrays without a magnetic field, (b) is grown arrays with a magnetic field applied perpendicular to the substrate, and (c) is grown arrays with a magnetic field applied parallel to the substrate. All samples were thinner than when grown in a 50 mL hydrothermal container because there was less precursor than in the 50 mL container. The growth of the rod was enhanced by a magnetic field. No difference in crystal orientation was observed irrespective of the direction in which the magnetic field was applied. In the case of the Czochralski method in a magnetic field, the convection of the melt is suppressed by the strong magnetic field, and the quality of the crystal is improved through improved temperature uniformity. In the present work, the growth of the ZnO rod could be promoted as the convection of the solution was suppressed by the application of the magnetic field and the temperature uniformity was improved. The orientation of ZnO did not change irrespective of the direction of the applied magnetic field, which may be attributed to the grain boundary energy of the crystal.

The magnetic energy per unit volume (U) of a diamagnetic material having a volume magnetic susceptibility of χ under the magnetic flux density (B) is given by the following Eq. 5,[56]

$$U = -\frac{\chi B^2}{2\mu_0}. \qquad \text{(Eq. 5)}$$

When the magnetic susceptibility has anisotropy, the difference between the magnetic energy of the easy and hard axes of magnetization is the anisotropic energy ΔU as shown in the following Eq. 6,

$$\Delta U = -\left(\chi_{easy} - \chi_{hard}\right)\frac{B^2}{2\mu_0} = -\Delta\chi\frac{B^2}{2\mu_0}. \qquad \text{(Eq. 6)}$$

Here, $\Delta\chi$ is magnetic anisotropy, χ_{easy} is the magnetic susceptibility of the easy axis of magnetization, and χ_{hard} is the magnetic susceptibility of the hard axis of magnetization.

The $\Delta\chi$ value of ZnO is required to calculate the orientation energy of ZnO under the magnetic field. However, the $\Delta\chi$ value of ZnO has not been reported. The magnetic susceptibilities of ZnO (-2.54×10^{-5}:SI system)[57] and Al_2O_3 (-8.93×10^{-5}:SI system) [58] are small and in the same order, so we may be able to use the absolute value of $\Delta\chi$ of Al_2O_3 as that of ZnO for the following discussion. Room temperature magnetic susceptibility is used in this discussion, as it was reported that the temperature dependence of magnetic susceptibility ($d\chi/dT$) of diamagnetic materials is quite small ($(d\chi/T)/\chi < 10^{-3}$ [K^{-1}]).[59] The $\Delta\chi$ of Al_2O_3 has been reported to be 5.28×10^{-9}. [58] Inserting the $\Delta\chi$ value of Al_2O_3 into Eq. 6 gives the magnetic anisotropy energy -3.02×10^{-27} [J/nm^3]. If the magnetic anisotropy energy of the nm-sized nucleus is larger than the grain boundary energy, epitaxial growth may be ignored and crystal growth in a direction different from that of the seed crystal may happen. The grain boundary energy of Al_2O_3 is reported to be about $0.19\times10^{-18} \sim 2.23\times10^{-18}$ [J/nm^2]. [60] Because the grain boundary energy is overwhelmingly larger than the magnetic anisotropy energy, epitaxial growth from the seed occurs regardless of the direction of magnetic field application.

Conclusion

Hexagonal plate ZnO particles were arranged regularly on an ITO glass substrate by optimizing the concentration of ZnO particles in the dip-coat solution and the withdrawal speed. The results of analysis by SEM and XRD showed that the c-axis of the ZnO crystal was perpendicular to the substrate. The high degree of orientation was characterized by the high Lotgering factor of 0.98. When the ZnO crystal was grown by hydrothermal synthesis using the obtained alignment film as a seed crystal, a ZnO rod could be homoepitaxially grown. The growth of the ZnO rod peaked in about 3 hours, and the film thickness increased from 200 nm to 1400 nm. When the precursor

concentration was low, rods with a hollow structure formed during hydrothermal synthesis, whereas rods with a solid structure were formed when the concentration was high. In hydrothermal synthesis in a magnetic field, we observed uniform rod growth due to the convective inhibition effect. The crystal orientation was unaffected by the application of an external magnetic field because the grain boundary energy exceeds the magnetic energy.

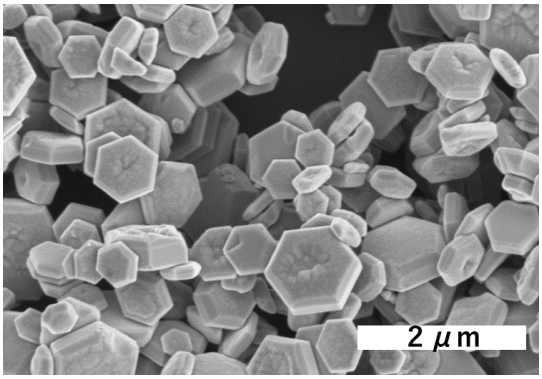

Figure 1. SEM image of hexagonal plate ZnO.

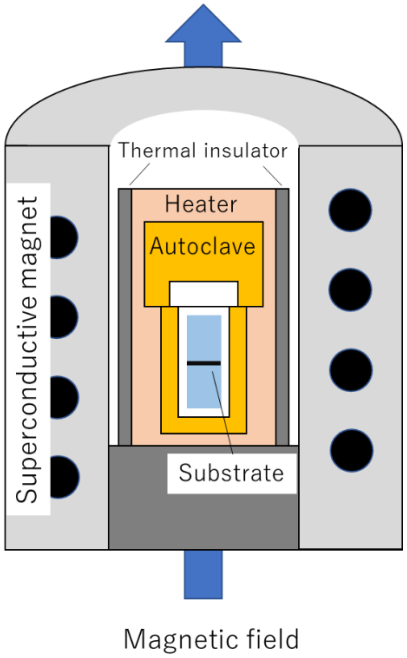

Figure 2. Illustration of hydrothermal treatment facility in a strong magnetic field.

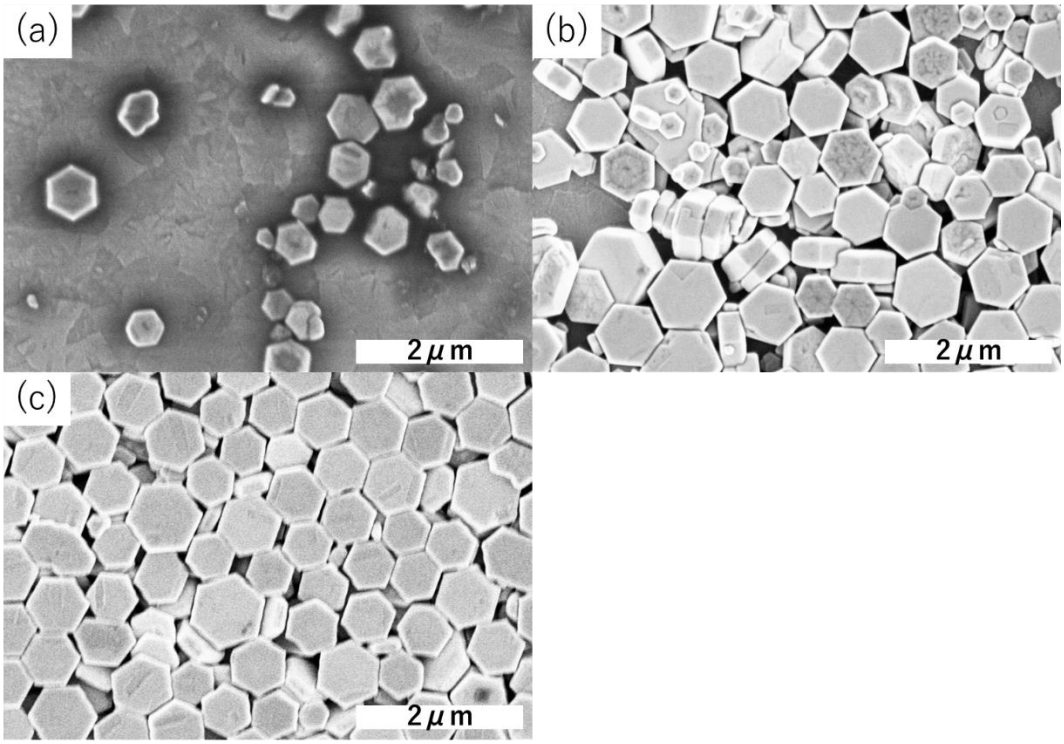

Figure 3. SEM images of ZnO arrays on ITO substrate fabricated from (a) 1 vol.%, (b) 7.5 vol.%, and (c) 10 vol.% suspensions.

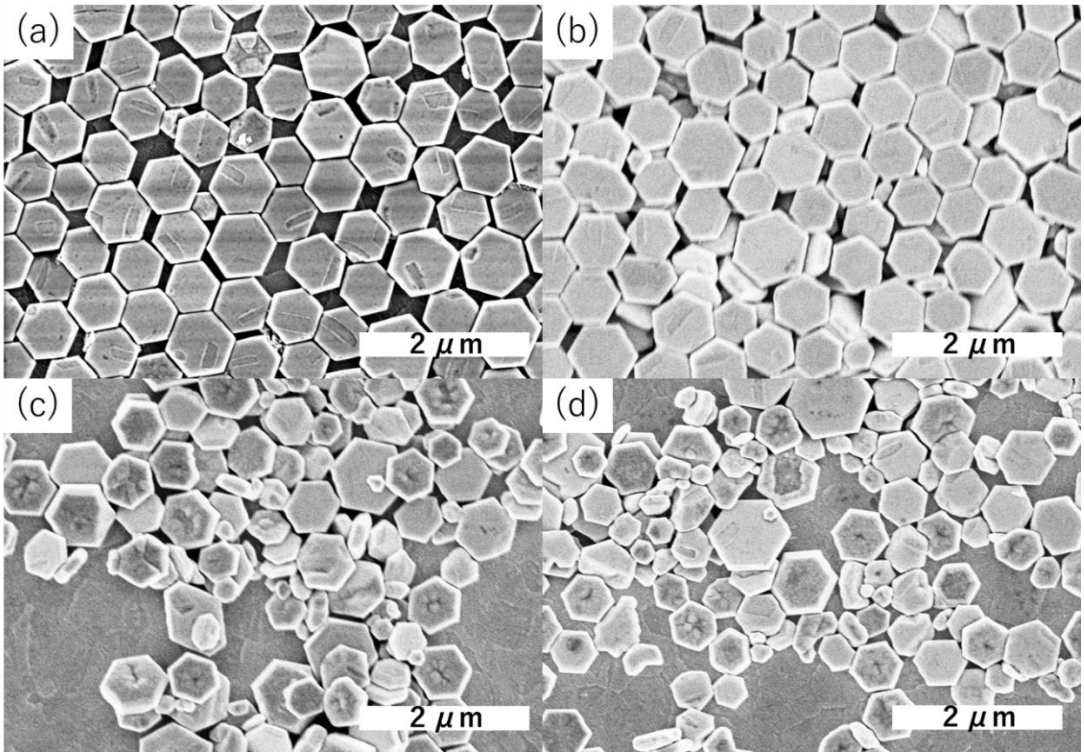

Figure 4. SEM images of ZnO arrays on ITO substrate fabricated by dip-coating with withdrawal speeds of (a) 5 μm/s, (b) 10 μm/s, (c) 100 μm/s, and (d) 1000 μm/s.

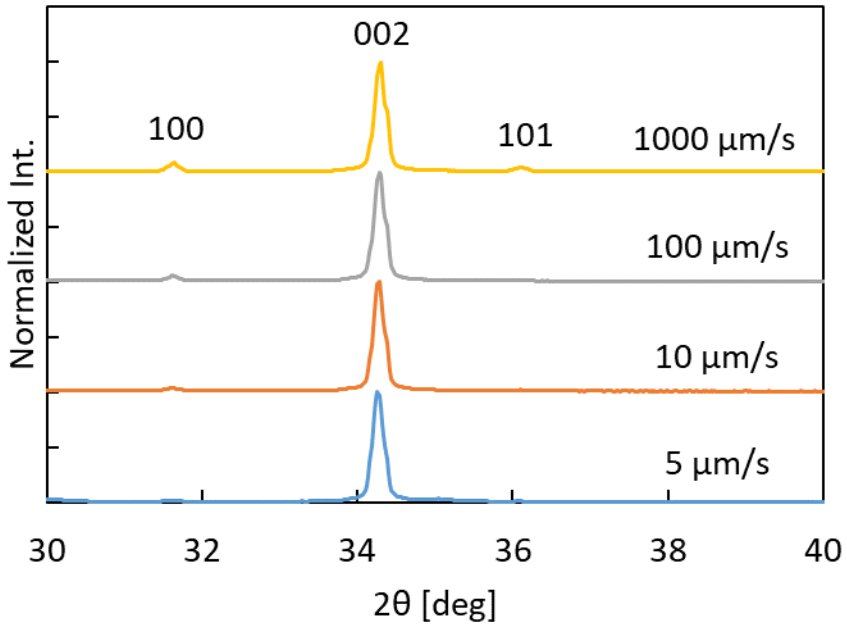

Figure 5. XRD patterns of dip-coated substrates with different withdrawal speeds.

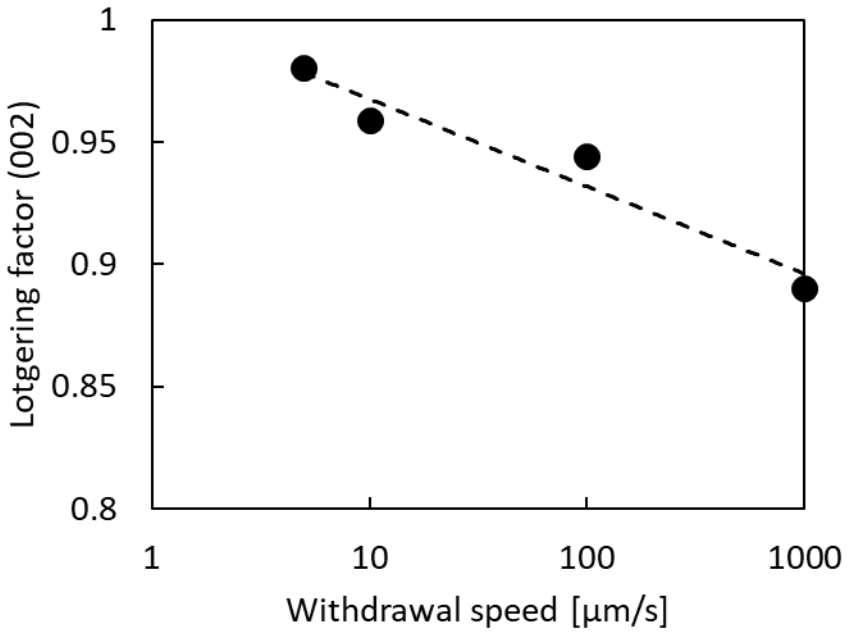

Figure 6. Lotgering factor obtained from XRD of the dip-coated substrate with different withdrawal speeds.

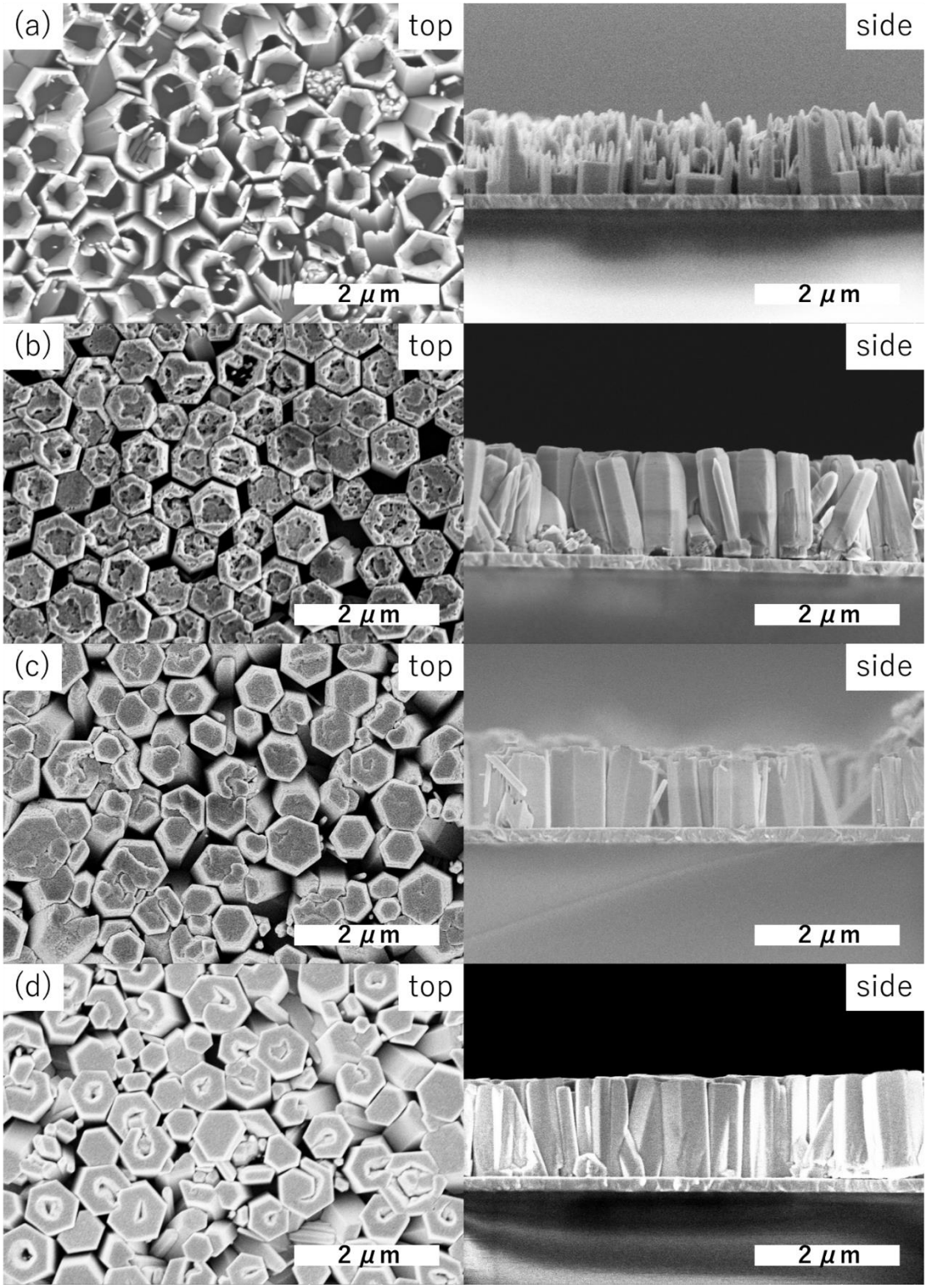

Figure 7. Top and side views of ZnO arrays grown by hydrothermal method for (a) 0.5 h, (b) 3 h, (c) 6 h, and (d) 12 h.

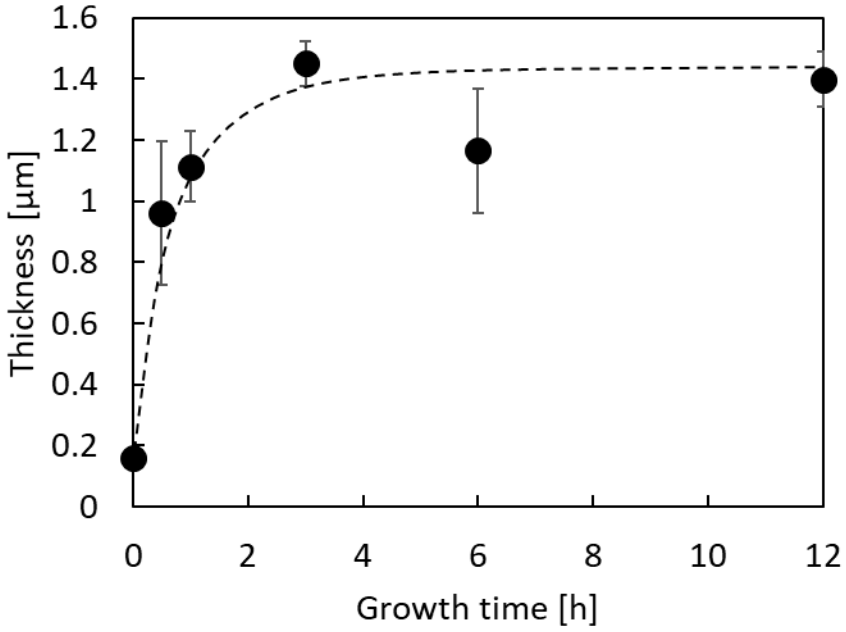

Figure 8. Dependence of ZnO film thickness on hydrothermal growth time.

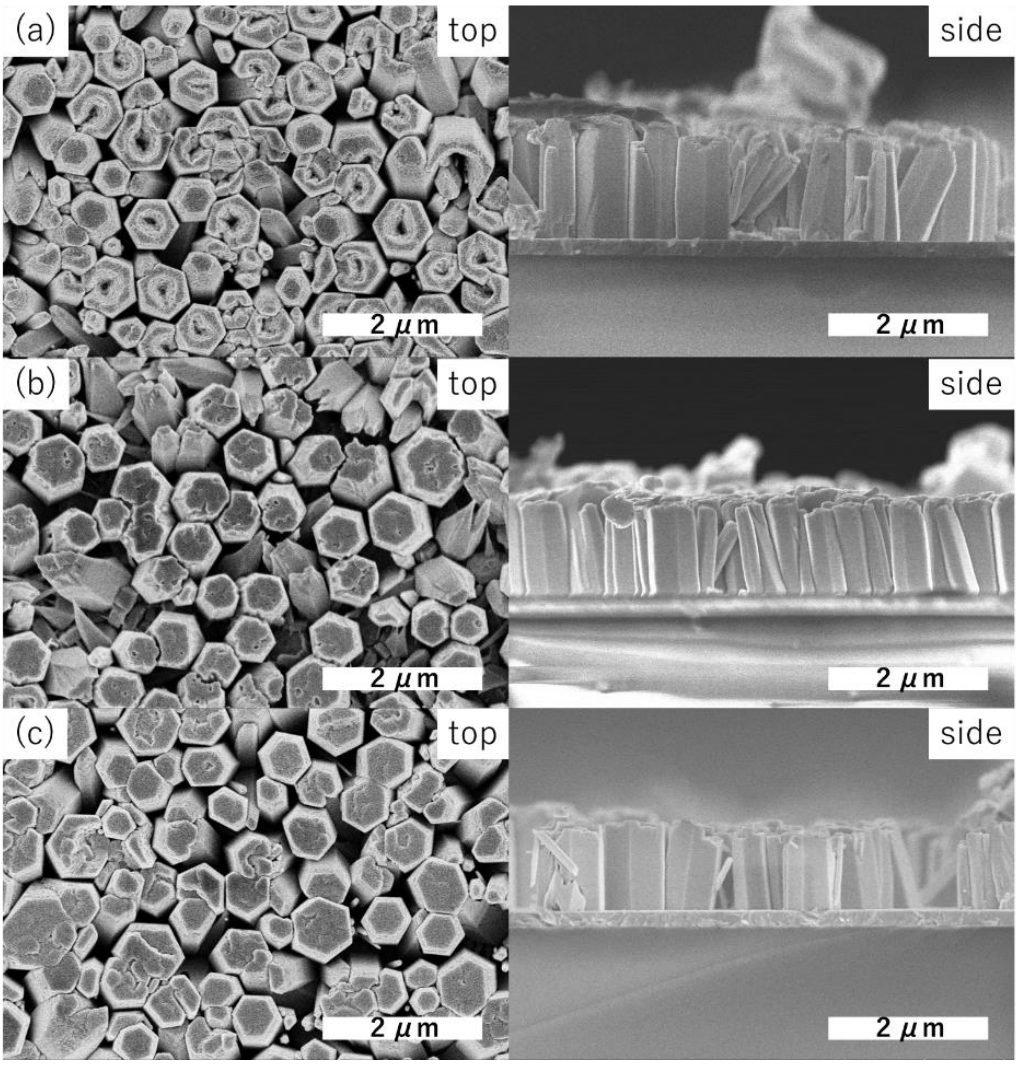

Figure 9. Top and side views of ZnO arrays grown by hydrothermal method with different precursor concentrations: (a) 0.02 mmol/L, (b) 0.05 mmol/L, (c) 0.1 mmol/L.

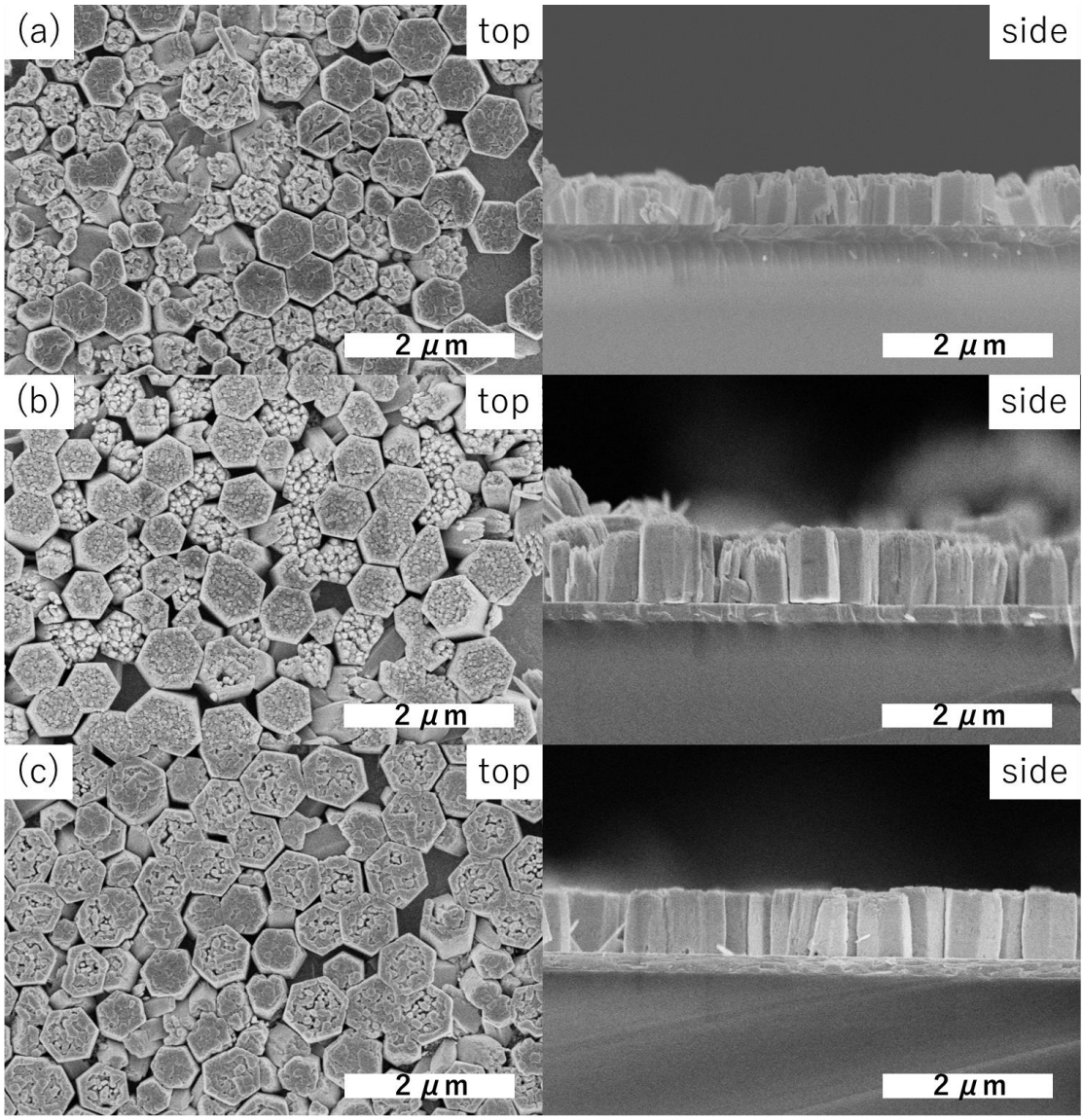

Figure 10. Top and side views of ZnO arrays grown by hydrothermal method with an external magnetic field: (a) No magnetic field, (b) magnetic field perpendicular to substrate, (c) magnetic field parallel to substrate.

ASSOCIATED CONTENT

Supporting Information.

The Supporting Information is available free of charge at,

https://pubs.acs.org/doi/10.1021/acs.langmuir.xxxxxxx.

XRD patterns (PDF)

AUTHOR INFORMATION

Corresponding Author

Takamasa Ishigaki - Department of Chemical Science and Technology, Hosei University, 3-7-2 Kajino-cho, Koganei, Tokyo 184-8584, Japan; Research Center for Micro-Nano Technology, 3-11-15 Midori-cho, Koganei, Tokyo 184-0003, Japan; orcid.org/ 0000-0002-7373-5708; E-mail: ishigaki@hosei.ac.jp

Authors

Satoshi Koyasu - Department of Chemical Science and Technology, Hosei University, 3-7-2 Kajino-cho, Koganei, Tokyo 184-8584, Japan

Hiroki Makino - Department of Chemical Science and Technology, Hosei University, 3-7-2 Kajino-cho, Koganei, Tokyo 184-8584, Japan

Naoki Tarutani - Graduate School of Advanced Science and Engineering, Hiroshima University, 1-4-1 Kagamiyama, Higashi-Hiroshima, Hiroshima 739-8527, Japan; Research Center for Micro-Nano Technology, 3-11-15 Midori-cho, Koganei, Tokyo 184-0003, Japan; orcid.org/ 0000-0003-0696-8082

Tohru Suzuki – Research Center for Functional Materials, National Institute for Materials Science (NIMS), 1-2-1 Sengen, Tsukuba, Ibaraki 305-0047, Japan

Tetsuo Uchikoshi - Research Center for Functional Materials, National Institute for Materials Science (NIMS), 1-2-1 Sengen, Tsukuba, Ibaraki 305-0047, Japan; orcid.org/ 0000-0003-3847-4781

Author Contributions

The manuscript was written through contributions of all authors. All authors have given approval to the final version of the manuscript.

Notes

The authors declare no competing financial interest.

REFERENCES

(1) Teke, A.; Özgür, Ü.; Doğan, S.; Gu, X.; Morkoç, H.; Nemeth, B.; Nause, J.; Everitt, H. O. Excitonic Fine Structure and Recombination Dynamics in Single-Crystalline ZnO. *Phys Rev B Condens Matter Mater Phys* **2004**, *70* (19), 1–10. https://doi.org/10.1103/PHYSREVB.70.195207/FIGURES/8/MEDIUM.

(2) Ohshima, E.; Ogino, H.; Niikura, I.; Maeda, K.; Sato, M.; Ito, M.; Fukuda, T. Growth of the 2-in-Size Bulk ZnO Single Crystals by the Hydrothermal Method. *J Cryst Growth* **2004**, *260* (1–2), 166–170. https://doi.org/10.1016/j.jcrysgro.2003.08.019.

(3) Carlotti, G.; Socino, G.; Petri, A.; Verona, E. Acoustic Investigation of the Elastic Properties of ZnO Films. *Appl Phys Lett* **1998**, *51* (23), 1889. https://doi.org/10.1063/1.98502.

(4) Emanetoglu, N. W.; Gorla, C.; Liu, Y.; Liang, S.; Lu, Y. Epitaxial ZnO Piezoelectric Thin Films for Saw Filters. *Mater Sci Semicond Process* **1999**, *2* (3), 247–252. https://doi.org/10.1016/S1369-8001(99)00022-0.

(5) Min-Yeol Choi, B.; Choi, D.; Jin, M.-J.; Kim, I.; Kim, S.-H.; Choi, J.-Y.; Yoon Lee, S.; Min Kim, J.; Kim, S.-W.; Choi, J.; Choi, D.; Lee, S. Y.; Kim, J. M.; Kim, S.; Choi, M.; Jin, M.; Kim, I.; Kim, S. Mechanically Powered Transparent Flexible Charge-Generating Nanodevices with Piezoelectric ZnO Nanorods. *Advanced Materials* **2009**, *21* (21), 2185–2189. https://doi.org/10.1002/ADMA.200803605.

(6) Maeda, K.; Sato, M.; Niikura, I.; Fukuda, T. Growth of 2 Inch ZnO Bulk Single Crystal by the Hydrothermal Method. *Semicond Sci Technol* **2005**, *20* (4), S49. https://doi.org/10.1088/0268-1242/20/4/006.

(7) Kaidashev, E. M.; Lorenz, M.; von Wenckstern, H.; Rahm, A.; Semmelhack, H. C.; Han, K. H.; Benndorf, G.; Bundesmann, C.; Hochmuth, H.; Grundmann, M. High Electron Mobility of Epitaxial ZnO Thin Films on C-Plane Sapphire Grown by Multistep Pulsed-Laser Deposition. *Appl Phys Lett* **2003**, *82* (22), 3901. https://doi.org/10.1063/1.1578694.
(8) Kato, H.; Sano, M.; Miyamoto, K.; Yao, T. Effect of O/Zn Flux Ratio on Crystalline Quality of ZnO Films Grown by Plasma-Assisted Molecular Beam Epitaxy. *Japanese Journal of Applied Physics, Part 1: Regular Papers and Short Notes and Review Papers* **2003**, *42* (4 B), 2241–2244. https://doi.org/10.1143/JJAP.42.2241/XML.
(9) Tsukazaki, A.; Ohtomo, A.; Kawasaki, M. High-Mobility Electronic Transport in ZnO Thin Films. *Appl Phys Lett* **2006**, *88* (15), 152106. https://doi.org/10.1063/1.2193727.
(10) Shelake, V.; Bhole, M. P.; Patil, D. S. Aluminium Doped Zinc Oxide Films as a Transparent Conducting Electrode for Organic Light Emitting Devices. *Optoelectronics and Advanced Materials, Rapid Communications* **2008**, *2* (6), 353–355. https://doi.org/10.1063/1.1605805.
(11) Oh, B. Y.; Jeong, M. C.; Moon, T. H.; Lee, W.; Myoung, J. M.; Hwang, J. Y.; Seo, D. S. Transparent Conductive Al-Doped ZnO Films for Liquid Crystal Displays. *J Appl Phys* **2006**, *99* (12). https://doi.org/10.1063/1.2206417.
(12) Chopra, K. L.; Major, S.; Pandya, D. K. Transparent Conductors—A Status Review. *Thin Solid Films* **1983**, *102* (1), 1–46. https://doi.org/10.1016/0040-6090(83)90256-0.
(13) Granqvist, C. G.; Hultåker, A. Transparent and Conducting ITO Films: New Developments and Applications. *Thin Solid Films* **2002**, *411* (1), 1–5. https://doi.org/10.1016/S0040-6090(02)00163-3.
(14) Moholkar, A. V.; Pawar, S. M.; Rajpure, K. Y.; Bhosale, C. H.; Kim, J. H. Effect of Fluorine Doping on Highly Transparent Conductive Spray Deposited Nanocrystalline Tin Oxide Thin Films. *Appl Surf Sci* **2009**, *255* (23), 9358–9364. https://doi.org/10.1016/j.apsusc.2009.07.035.
(15) Fukano, T.; Motohiro, T. Low-Temperature Growth of Highly Crystallized Transparent Conductive Fluorine-Doped Tin Oxide Films by Intermittent Spray Pyrolysis Deposition. *Solar Energy Materials and Solar Cells* **2004**, *82* (4), 567–575. https://doi.org/10.1016/j.solmat.2003.12.009.
(16) Shanthi, S.; Subramanian, C.; Ramasamy, P. Preparation and Properties of Sprayed Undoped and Fluorine Doped Tin Oxide Films. *Materials Science and Engineering B* **1999**, *57* (2), 127–134. https://doi.org/10.1016/S0921-5107(98)00314-6.
(17) Kalyanaraman, S.; Thangavel, R.; Vettumperumal, R. High Mobility Formation of P-Type Al Doped ZnO:N Films Annealed under NH3 Ambient. *Journal of Physics and Chemistry of Solids* **2013**, *74* (3), 504–508. https://doi.org/10.1016/j.jpcs.2012.11.019.
(18) Shen, H. L.; Zhang, H.; Lu, L. F.; Jiang, F.; Yang, C. Preparation and Properties of AZO Thin Films on Different Substrates. *Progress in Natural Science: Materials International* **2010**, *20* (1), 44–48. https://doi.org/10.1016/S1002-0071(12)60005-7.
(19) Fortunato, E. M. C.; Barquinha, P. M. C.; Pimentel, A. C. M. B. G.; Gonçalves, A. M. F.; Marques, A. J. S.; Martins, R. F. P.; Pereira, L. M. N. Wide-Bandgap High-Mobility ZnO Thin-Film Transistors Produced at Room Temperature. *Appl Phys Lett* **2004**, *85* (13), 2541. https://doi.org/10.1063/1.1790587.
(20) Zhang, Y.; Kan, Y.; Gao, K.; Gu, M.; Shi, Y.; Zhang, X.; Xue, Y.; Zhang, X.; Liu, Z.; Zhang, Y.; Yuan, J.; Ma, W.; Jen, A. K. Y. Hybrid Quantum Dot/Organic Heterojunction:

A Route to Improve Open-Circuit Voltage in PbS Colloidal Quantum Dot Solar Cells. *ACS Energy Lett* **2020**, *5* (7), 2335–2342. https://doi.org/10.1021/acsenergylett.0c01136.
(21) Repins, I.; Contreras, M. A.; Egaas, B.; DeHart, C.; Scharf, J.; Perkins, C. L.; To, B.; Noufi, R. 19.9%-Efficient ZnO/CdS/ CuInGaSe2 Solar Cell with 81.2% Fill Factor. *Progress in Photovoltaics Research and Applications* **2008**, *16* (3), 253–239. https://doi.org/10.1002/pip.
(22) Hongsith, N.; Viriyaworasakul, C.; Mangkorntong, P.; Mangkorntong, N.; Choopun, S. Ethanol Sensor Based on ZnO and Au-Doped ZnO Nanowires. *Ceram Int* **2008**, *34* (4), 823–826. https://doi.org/10.1016/J.CERAMINT.2007.09.099.
(23) Franco, M. A.; Conti, P. P.; Andre, R. S.; Correa, D. S. A Review on Chemiresistive ZnO Gas Sensors. *Sensors and Actuators Reports* **2022**, *4*, 100100. https://doi.org/10.1016/J.SNR.2022.100100.
(24) Gao, T.; Wang, T. H. Synthesis and Properties of Multipod-Shaped ZnO Nanorods for Gas-Sensor Applications. *Applied Physics A 2004 80:7* **2004**, *80* (7), 1451–1454. https://doi.org/10.1007/S00339-004-3075-2.
(25) Watson, J. The Tin Oxide Gas Sensor and Its Applications. *Sensors and Actuators* **1984**, *5* (1), 29–42. https://doi.org/10.1016/0250-6874(84)87004-3.
(26) Darvishnejad, M. H.; Anaraki Firooz, A.; Beheshtian, J.; Khodadadi, A. A. Highly Sensitive and Selective Ethanol and Acetone Gas Sensors by Adding Some Dopants (Mn, Fe, Co, Ni) onto Hexagonal ZnO Plates. *RSC Adv* **2016**, *6* (10), 7838–7845. https://doi.org/10.1039/c5ra24169c.
(27) Peng, W.; Qu, S.; Cong, G.; Wang, Z. Synthesis and Structures of Morphology-Controlled ZnO Nano-and Microcrystals. **2006**. https://doi.org/10.1021/cg0505261.
(28) Li, G. R.; Hu, T.; Pan, G. L.; Yan, T. Y.; Gao, X. P.; Zhu, H. Y. Morphology-Function Relationship of ZnO: Polar Planes, Oxygen Vacancies, and Activity. *Journal of Physical Chemistry C* **2008**, *112* (31), 11859–11864. https://doi.org/10.1021/JP8038626/SUPPL_FILE/JP8038626-FILE002.PDF.
(29) Zhang, J.; Sun, L.; Yin, J.; Su, H.; Liao, C.; Yan, C. Control of ZnO Morphology via a Simple Solution Route. *Chemistry of Materials* **2002**, *14* (10), 4172–4177. https://doi.org/10.1021/CM020077H/ASSET/IMAGES/LARGE/CM020077HF00007.JPEG.
(30) Cheng, H. M.; Hsu, H. C.; Chen, S. L.; Wu, W. T.; Kao, C. C.; Lin, L. J.; Hsieh, W. F. Efficient UV Photoluminescence from Monodispersed Secondary ZnO Colloidal Spheres Synthesized by Sol-Gel Method. *J Cryst Growth* **2005**, *277* (1–4), 192–199. https://doi.org/10.1016/j.jcrysgro.2004.12.133.
(31) Jung, S. H.; Oh, E.; Lee, K. H.; Yang, Y.; Park, C. G.; Park, W.; Jeong, S. H. Sonochemical Preparation of Shape-Selective ZnO Nanostructures. *Cryst Growth Des* **2008**, *8* (1), 265–269. https://doi.org/10.1021/CG070296L/SUPPL_FILE/CG070296L-FILE002.PDF.
(32) Shoaee, S.; Briscoe, J.; Durrant, J. R.; Dunn, S.; Shoaee, S.; Durrant, R.; Briscoe, J.; Dunn, S. Acoustic Enhancement of Polymer/ZnO Nanorod Photovoltaic Device Performance. *Advanced Materials* **2014**, *26* (2), 263–268. https://doi.org/10.1002/ADMA.201303304.
(33) Olson, D. C.; Lee, Y. J.; White, M. S.; Kopidakis, N.; Shaheen, S. E.; Ginley, D. S.; Voigt, J. A.; Hsu, J. W. P. Effect of Polymer Processing on the Performance of Poly(3-Hexylthiophene)/ ZnO Nanorod Photovoltaic Devices. *Journal of Physical Chemistry C*

2007, *111* (44), 16640–16645. https://doi.org/10.1021/JP0757816/ASSET/IMAGES/LARGE/JP0757816F00007.JPEG.
(34) Ravirajan, P.; Peiró, A. M.; Nazeeruddin, M. K.; Graetzel, M.; Bradley, D. D. C.; Durrant, J. R.; Nelson, J. Hybrid Polymer/Zinc Oxide Photovoltaic Devices with Vertically Oriented ZnO Nanorods and an Amphiphilic Molecular Interface Layer. *Journal of Physical Chemistry B* **2006**, *110* (15), 7635–7639. https://doi.org/10.1021/JP0571372/ASSET/IMAGES/LARGE/JP0571372F00003.JPEG.
(35) Xu, Y.; Liu, T.; Li, Z.; Feng, B.; Li, S.; Duan, J.; Ye, C.; Zhang, J.; Wang, H. Preparation and Photovoltaic Properties of Perovskite Solar Cell Based on ZnO Nanorod Arrays. *Appl Surf Sci* **2016**, *388*, 89–96. https://doi.org/10.1016/J.APSUSC.2016.03.079.
(36) Kartopu, G.; Turkay, D.; Ozcan, C.; Hadibrata, W.; Aurang, P.; Yerci, S.; Unalan, H. E.; Barrioz, V.; Qu, Y.; Bowen, L.; Gürlek, A. K.; Maiello, P.; Turan, R.; Irvine, S. J. C. Photovoltaic Performance of CdS/CdTe Junctions on ZnO Nanorod Arrays. *Solar Energy Materials and Solar Cells* **2018**, *176*, 100–108. https://doi.org/10.1016/J.SOLMAT.2017.11.036.
(37) Huang, M. H.; Wu, Y.; Feick, H.; Tran, N.; Weber, E.; Yang, P. Catalytic Growth of Zinc Oxide Nanowires by Vapor Transport. *Advanced Materials* **2001**, *13* (2), 113–116. https://doi.org/https://doi.org/10.1002/1521-4095(200101)13:2<113::AID-ADMA113>3.0.CO;2-H.
(38) Olson, D. C.; Shaheen, S. E.; Collins, R. T.; Ginley, D. S. The Effect of Atmosphere and ZnO Morphology on the Performance of Hybrid Poly(3-Hexylthiophene)/ZnO Nanofiber Photovoltaic Devices. *Journal of Physical Chemistry C* **2007**, *111* (44), 16670–16678. https://doi.org/10.1021/JP0734225/ASSET/IMAGES/LARGE/JP0734225F00015.JPEG.
(39) Wong, S.; Kitaev, V.; Ozin, G. A. Colloidal Crystal Films: Advances in Universality and Perfection. *J Am Chem Soc* **2003**, *125* (50), 15589–15598. https://doi.org/10.1021/JA0379969/SUPPL_FILE/JA0379969SI20031001_054830.PDF.
(40) Zhang, J.-T.; Wang, L.; Lamont, D. N.; Velankar, S. S.; Asher, S. A. Fabrication of Large-Area Two-Dimensional Colloidal Crystals. *Angewandte Chemie* **2012**, *124* (25), 6221–6224. https://doi.org/10.1002/ange.201105439.
(41) Kralchevsky, P. A.; Paunov, V. N.; Denkov, N. D.; Nagayama, K. Capillary Image Forces: I. Theory. *J Colloid Interface Sci* **1994**, *167* (1), 47–65. https://doi.org/10.1006/JCIS.1994.1332.
(42) Velev, O. D.; Denkov, N. D.; Paunov, V. N.; Kralchevsky, P. A.; Nagayama, K. Capillary Image Forces: II. Experiment. *J Colloid Interface Sci* **1994**, *167* (1), 66–73. https://doi.org/10.1006/JCIS.1994.1333.
(43) Fang, M.; Liu, Z. W. Controllable Size and Photoluminescence of ZnO Nanorod Arrays on Si Substrate Prepared by Microwave-Assisted Hydrothermal Method. *Ceram Int* **2017**, *43* (9), 6955–6962. https://doi.org/10.1016/J.CERAMINT.2017.02.119.
(44) Baruah, S.; Dutta, J. Effect of Seeded Substrates on Hydrothermally Grown ZnO Nanorods. *J Solgel Sci Technol* **2009**, *50* (3), 456–464. https://doi.org/10.1007/S10971-009-1917-2/FIGURES/12.
(45) Feng, Y.; Zhang, M.; Guo, M.; Wang, X. Studies on the PEG-Assisted Hydrothermal Synthesis and Growth Mechanism of ZnO Microrod and Mesoporous Microsphere Arrays on the Substrate. *Cryst Growth Des* **2010**, *10* (4), 1500–1507. https://doi.org/10.1021/CG900327V/ASSET/IMAGES/LARGE/CG-2009-00327V_0014.JPEG.

(46) Wu, W.; Hu, G.; Cui, S.; Zhou, Y.; Wu, H. Epitaxy of Vertical ZnO Nanorod Arrays on Highly (001)-Oriented ZnO Seed Monolayer by a Hydrothermal Route. *Cryst Growth Des* **2008**, *8* (11), 4014–4020. https://doi.org/10.1021/CG800210M/SUPPL_FILE/CG800210M_SI_001.PDF.
(47) Hoshikawa, K. Czochralski Silicon Crystal Growth in the Vertical Magnetic Field. *Jpn J Appl Phys* **1982**, *21* (9), L545–L547. https://doi.org/10.1143/JJAP.21.L545/XML.
(48) Sazaki, G.; Durbin, S. D.; Miyashita, S.; Ujihara, T.; Nakajima, K.; Motokawa, M. Magnetic Damping of the Temperature-Driven Convection in NaCl Aqueous Solution Using a Static and Homogeneous Field of 10 T. *Japanese Journal of Applied Physics, Part 2: Letters* **1999**, *38* (7 B), L842. https://doi.org/10.1143/JJAP.38.L842/XML.
(49) Tanaka, S.; Makiya, A.; Kato, Z.; Uchida, N.; Kimura, T.; Uematsu, K. Fabrication of C-Axis Oriented Polycrystalline ZnO by Using a Rotating Magnetic Field and Following Sintering. *Journal of Materials Research 2006 21:3* **2006**, *21* (3), 703–707. https://doi.org/10.1557/JMR.2006.0098.
(50) Sugiyama, T.; Tahashi, M.; Sassa, K.; Asai, S. The Control of Crystal Orientation in Non-Magnetic Metals by Imposition of a High Magnetic Field. *ISIJ International* **2003**, *43* (6), 855–861. https://doi.org/10.2355/ISIJINTERNATIONAL.43.855.
(51) Dimitrov, A. S.; Nagayama, K. Continuous Convective Assembling of Fine Particles into Two-Dimensional Arrays on Solid Surfaces. *Langmuir* **1996**, *12* (5), 1303–1311. https://doi.org/10.1021/LA9502251.
(52) Lotgering, F. K. Topotactical Reactions with Ferrimagnetic Oxides Having Hexagonal Crystal Structures—I. *Journal of Inorganic and Nuclear Chemistry* **1959**, *9* (2), 113–123. https://doi.org/10.1016/0022-1902(59)80070-1.
(53) Desarnaud, J.; Derluyn, H.; Carmeliet, J.; Bonn, D.; Shahidzadeh, N. Hopper Growth of Salt Crystals. *Journal of Physical Chemistry Letters* **2018**, *9* (11), 2961–2966. https://doi.org/10.1021/ACS.JPCLETT.8B01082/SUPPL_FILE/JZ8B01082_SI_001.PDF.
(54) Iwanaga, H.; Shibata, N. Growth Mechanism of Hollow ZnO Crystals from ZnSe. *J Cryst Growth* **1974**, *24–25* (C), 357–361. https://doi.org/10.1016/0022-0248(74)90335-2.
(55) Mullins, W. W.; Sekerka, R. F. Stability of a Planar Interface During Solidification of a Dilute Binary Alloy. *J Appl Phys* **2004**, *35* (2), 444. https://doi.org/10.1063/1.1713333.
(56) Simon, M. D.; Geim, A. K. Diamagnetic Levitation: Flying Frogs and Floating Magnets (Invited). *J Appl Phys* **2000**, *87* (9), 6200. https://doi.org/10.1063/1.372654.
(57) Lal, R. B. Magnetic Susceptibility of Group II, Group VI Semiconductor ZnO. *Solid State Commun* **1966**, *4* (10), 529–531. https://doi.org/10.1016/0038-1098(66)90418-2.
(58) Uyeda, C.; Tsuchiyama, A.; Yamanaka, T.; Date, M. Field-Induced Oscillation and Rotation of Diamagnetic Oxide Crystals. *Physics and Chemistry of Minerals 1993 20:2* **1993**, *20* (2), 82–85. https://doi.org/10.1007/BF00207199.
(59) Hudgens, S.; Kastner, M.; Fritzsche, H. Diamagnetic Susceptibility of Tetrahedral Semiconductors. *Phys Rev Lett* **1974**, *33* (26), 1552. https://doi.org/10.1103/PhysRevLett.33.1552.
(60) Suzuki, H.; Matsubara, H.; Kishino, J.; Kondoh, T. Simulation of Surface and Grain Boundary Properties of Alumina by Molecular Dynamics Method. *Journal of the Ceramic Society of Japan* **1998**, *106* (1240), 1215–1222. https://doi.org/10.2109/JCERSJ.106.1215.

Table of Contents Graphic (TOC)